

Tl⁺-like phosphors. It is striking that this mechanism applies for two opposite physical situations, Jahn-Teller coupling larger or smaller than spin-orbit coupling. The importance of the hyperfine interaction in the dynamics of the emission has also been illustrated by recent studies of the polarization of the emission under polarized excitation light.¹² The knowledge of the hyperfine interaction and of the Jahn-Teller coupling in the excited states ³T₁ is now good enough to devise a scheme for nuclear orientation by optical pumping as was done years ago for mercury vapor.²²

The Laboratoire de Spectrométrie Physique is a Laboratoire associé au Centre National de la Recherche Scientifique.

^(a)Present address: Sherman Fairchild Laboratory No. 161, Lehigh University, Bethlehem, Penn. 18015.

¹W. B. Fowler, in *Physics of Color Centers*, edited by W. B. Fowler (Academic, New York, 1968), p. 54.

²W. B. Fowler, *Phys. Status Solidi* **33**, 763 (1969).

³A. Fukuda, *Phys. Rev. B* **1**, 4161 (1970).

⁴A. E. Hughes and G. P. Pells, *Phys. Status Solidi* (b) **71**, 707 (1975).

⁵M. P. Fontana, G. Viliani, M. Bacci, and A. Ranfagni, *Solid State Commun.* **18**, 1615 (1976).

⁶F. S. Ham, *Phys. Rev.* **138**, A1727 (1965).

⁷A. Ranfagni, *Phys. Rev. Lett.* **28**, 743 (1972); M. Bacci, A. Ranfagni, M. Cetica, and G. Viliani, *Phys. Rev. B* **12**, 5907 (1975).

⁸Le Si Dang, R. Romestain, Y. Merle d'Aubigné, and

A. Fukuda, *Phys. Rev. Lett.* **38**, 1539 (1977).

⁹Le Si Dang, Y. Merle d'Aubigné, R. Romestain, and A. Fukuda, *Solid State Commun.* **26**, 413 (1978).

¹⁰A. Fukuda and P. Yuster, *Phys. Rev. Lett.* **28**, 1032 (1972); D. Simkin, J. P. Martin, Le Si Dang, and Y. Kamishina, to be published.

¹¹P. Edel, C. Hennies, Y. Merle d'Aubigné, R. Romestain, and Y. Twarowski, *Phys. Rev. Lett.* **28**, 1268 (1972).

¹²Le Si Dang, Y. Merle d'Aubigné, and R. Romestain, *J. Lumin.* **18/19**, 331 (1979).

¹³W. B. Fowler, M. J. Marrone, and M. N. Kabler, *Phys. Rev. B* **8**, 5909 (1973).

¹⁴D. Klick and H. G. Drickamer, *Phys. Rev. B* **17**, 952 (1978).

¹⁵Le Si Dang, R. Romestain, D. Simkin, and A. Fukuda, *Phys. Rev. B* **18**, 2989 (1978).

¹⁶R. Illingworth, *Phys. Rev.* **136**, A508 (1964); M. F. Trinkler and I. K. Plyavin, *Phys. Status Solidi* **11**, 277 (1965); S. Benci, M. P. Fontana, and M. Manfredi, *Solid State Commun.* **18**, 1423 (1976).

¹⁷P. G. Baranov and V. A. Khrantsov, *Fiz. Tverd. Tela* **20**, 1870 (1978) [*Sov. Phys. Solid State* **20**, 1080 (1978)].

¹⁸A. Raüber and J. Schneider, *Phys. Status Solidi* **18**, 125 (1966).

¹⁹R. C. Du Varney and A. K. Garrison, *Phys. Rev. B* **12**, 10 (1975).

²⁰W. Dreybrodt and D. Silber, *Phys. Status Solidi* **20**, 337 (1967).

²¹E. Werkmann, R. Huss, W. Frey, and H. Seidel, in *Proceedings of the International Conference on Color Centers in Ionic Crystals*, Sendai, Japan, 1974 (unpublished).

²²B. Cagnac, J. Brossel, and A. Kastler, *C. R. Acad. Sci.* **246**, 1827 (1958).

KH₂PO₄ in a Field: A Transition without Critical Microscopic Fluctuations

Eric Courtens, Robert Gammon,^(a) and Shlomo Alexander^(b)

IBM Zurich Research Laboratory, 8803 Ruschlikon, Switzerland

(Received 2 July 1979)

Light scattering on potassium dihydrogen phosphate demonstrates that the ordering electric field reduces the isothermal microscopic response. At the continuous transition occurring at the critical field no microscopic critical fluctuation exists (no diverging correlation range) and only macroscopic thermodynamic quantities can diverge classically. This general effect for symmetry-nonbreaking elastic transitions is caused in potassium dihydrogen phosphate by higher than bilinear strain-polarization couplings in the free energy.

Potassium dihydrogen phosphate (KDP) (KH₂PO₄) experiences a slightly discontinuous paraelectric (PE) to ferroelectric (FE) transition at $T_{tr} \approx 122$ K.¹ The ferroelectric mode softens towards the extrapolated clamped Curie temperature T_C .

The noncentrosymmetric PE phase (point group $\bar{4}2m$) has a nonzero h_{63} piezoelectric constant which couples the polarization $P_3 \equiv P$ to the e_6 shear strain. This produces a soft elastic branch with stability limit at the extrapolated free Curie

temperature T_a , $T_a - T_C \approx 4.5$ K.² The elastic transition generates an orthorhombic ($2mm$) FE phase. Under application of a static electric field E parallel to the c axis, P is induced in the PE phase and, via h_{63} , an orthorhombic distortion results: The PE-to-FE transition becomes *symmetry nonbreaking*. As E increases, the polarization discontinuity at the transition decreases until an ordinary critical point (T_K, E_K) is reached at which the transition becomes continuous and the coexistence curve terminates (inset of Fig. 1).³ The present Letter reports static and dynamic light-scattering results obtained in this region of the (T, E) plane, uncovering a number of novel features of the elastic instability. The symmetry-allowed distortions $e_1 = e_2$ and e_3 , all of order P^2 ,⁴ usually not included in the Landau free-energy expansion,⁵ are found to be essential, not only to a quantitative description of the scattered intensity as described below, but also to a *qualitative* understanding of the nature of the instability. At K there is no *microscopic* critical fluctuation (no critical spatial Fourier component of finite \vec{q}), and hence no opalescence. Our results constitute the first experimental demonstration of fluctuation quenching in a Cowley type-0 transition.⁶

The measurements were performed on a high-quality annealed sample for which the static central peak (CP) intensity was, at most, a few per-

cent of the dynamic scattering at all T and E in the region of interest.⁷ The observation geometry was the usual one in which the soft shear phonon propagating along \hat{x} scatters in a narrow cone about the $\hat{x} - \hat{z}$ direction.⁵ The z faces of the crystal were Cr-Au plated. The field polarity was switched adiabatically every 5 sec to 2 min, depending on the measurement, in order to prevent uncertain field distributions caused by injected charges. During switching, adiabatic cooling followed by heating took place,¹ indicated by a scattering flash. This produced no detectable aftereffects, whereas at each new field *magnitude* it was necessary to wait for thermalization.¹ The temperature was stabilized to better than 1 mK. The values used here are all referenced to the extrapolated T_a which was derived from fitting the sample dielectric constant measured *in situ* by a Curie law. A similar fit of the integrated scattered intensity at $E = 0$ gave the same T_a to better than 3 mK. The spectral measurements were performed as previously described,⁷ Intensity measurements were made with a collection hole limiting the acceptance angle, and an image hole of ~ 1 mm limiting the lateral extent of the scattering volume. The scattered light was phot counted and normalized to the laser intensity transmitted by the sample by use of a digital divider.

Brillouin spectra obtained at $T - T_a = 106$ mK and at various fields are presented in Fig. 1. At zero field, and with this proximity to the transition, the phonon is almost overdamped giving a single-peak appearance. A small static CP carries only 1% of the integrated intensity, as revealed by fitting.⁷ As E increases, three features are immediately apparent: a CP grows, the phonon frequency moves up, and the integrated intensity decreases. The field-induced CP is dynamic, with a width ~ 100 MHz, whereas the static component does not change appreciably with E . The latter point can be checked with use of a magnifier: The laser-illuminated static scattering centers can then be resolved, and no appreciable field dependence is seen. The *spectral* features can be *qualitatively* explained within the usual Landau theory. In the presence of E , temperature and polarization fluctuations couple via the mixed second derivative of the Gibbs free energy, $\partial^2 G / \partial P \partial T \propto P$. A heat-diffusion CP results,⁸ and the remaining spectral response is adiabatic, causing an increase of the observed phonon frequency. The isothermal response, however, is the integral of the spectrum, and it is

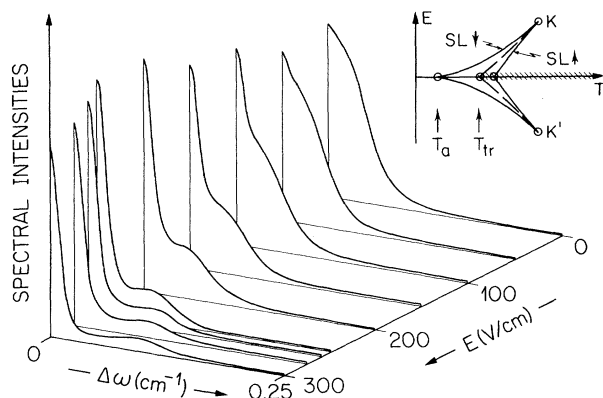


FIG. 1. Half-free-spectral range of Fabry-Perot spectra. The inset shows the phase diagram, with the thermodynamic transition line (broken) and the stability limits for the up (SL \uparrow) and down (SL \downarrow) transitions; the symmetry is $2mm$ in the whole plane, except along the hatched line, where it is $\bar{4}2m$. The spectra shown are taken at a temperature presumably close to T_K ($T - T_a = 106$ mK), with E_K between ~ 200 and 300 V/cm (Ref. 3).

not modified by the above coupling⁹; its *decrease* is thus surprising. Naively one would anticipate an intensity increase as one approaches the critical point K . This is also predicted by the usual Landau theory. In fact, to explain our results, it is necessary to include in the free energy *all* elastic terms to order P^4 , as shown below. Then a *quantitative* account of the spectra also requires a more careful treatment, as the necessary improvements of the Landau theory mix into the wave-propagation problem elastic constants other than C_{66} .

The intensity $I(T, E)$ scattered from fluctuations in the $(1, 0, 0)$ direction is proportional to the corresponding static response $\langle \delta P_{\bar{q}} \delta P_{\bar{q}} \rangle$. It was measured with an acceptance angle narrower than the scattering cone centered on it with $E = 0$. The inverse intensity can be parametrized in a way suggested by the Landau expansion,⁵

$$I^{-1} \propto a(T - T_a) + 3B_m P^2 + O(P^4), \quad (1)$$

but with $B_m > 0$. Using the equation of state $E = a(T - T_a)P + O(P^3)$, where $a = 3.9 \times 10^{-3}$ esu/K,³ one obtains

$$\frac{I(T, E=0)}{I(T, E)} = 1 + 3B_m \frac{E^2}{a^3(T - T_a)^3} + O(E^4). \quad (2)$$

This allows one to present as a function of the scaled field squared, $E^2/a^3(T - T_a)^3$, the intensities obtained at all temperatures (Fig. 2). The points were fitted by a parabola although the scaling does not strictly apply to $O(E^4)$; B_m is then given by the initial slope as shown.

The field also modifies the direction of the

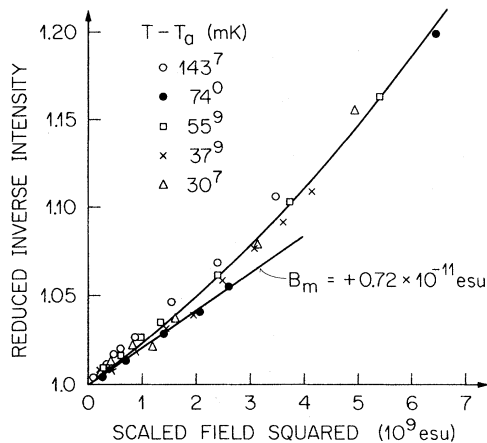


FIG. 2. Scattered intensity data with parabolic fit and initial slope.

scattering cone. This is easily observed with the eye slightly above the horizontal (x, z) scattering plane: The scattered intensity is seen to depend on the sign of E . The sign reverses when the eye is placed below the plane, indicating a vertical shift of the scattering cone proportional to E . We verified that crystal optics makes a negligible contribution to this effect. Hence it indicates a motion of the *softest* direction out of the scattering plane. To measure it, a 2.5-mrad collection aperture was moved along \hat{y} , selecting a scattering direction θ , and the values $I_0(\theta)$ at $E = 0$, $I_+(\theta)$ with $E > 0$, and $I_-(\theta)$ with $E < 0$, were obtained. To minimize the influence of accidental optical defects in the collection path (such as scratches on the crystal faces) the results are expressed in terms of a dimensionless ratio, the most convenient one being $R = (I_-^{-1} - I_+^{-1}) / 2I_0^{-1}$ (Fig. 3). At $\theta = 0$, the slope $S(E)$ is obtained from the straight-line fits. These slopes divided by E are shown in the inset. In summary, the scattered intensity decreases under field, and its direction of maximum moves off \hat{x} towards \hat{y} .

To account for these results *all* three orthorhombic strains e_1^0 , e_2^0 , and e_3^0 , have to be included since they transform as the identity representation and are thus active in the transition. The corresponding tetragonal strains result from a rotation by 45° about z .¹⁰ They are $e_1 = e_2 = (e_1^0 + e_2^0)/2$, $e_3 = e_3^0$, and $e_6 = e_2^0 - e_1^0$. The Gibbs free energy $G(T, P, E, e_i, \sigma_i)$ is, in general, a function of all strains e_i and stresses σ_i . A consistent expansion must include all symmetry-allowed terms to $O(P^4)$, i.e., all electrostrictive and

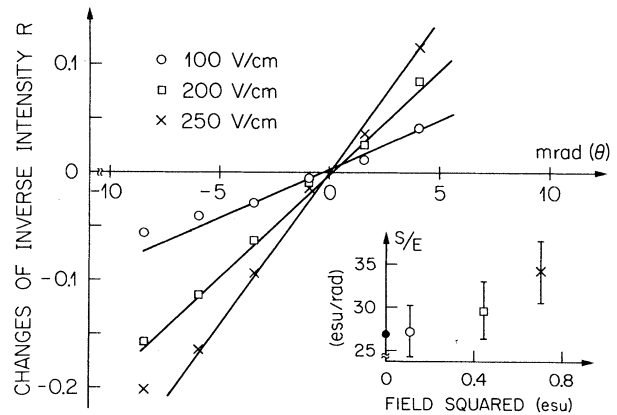


FIG. 3. $R(\theta)$ for three values of E and with $T - T_a = 106$ mK. The straight lines are best fits whose slopes divided by E are shown in the inset, the full point being the calculated value.

higher-order elastic constants. The statics of the free crystal is then obtained by minimization, $\partial G/\partial e_i = 0$, from which the e_i 's are extracted and introduced in $\partial G/\partial P = 0$. This gives an equation of state $E = a(T - T_a)P + B_M P^3 + O(P^5)$, with an explicit expression for B_M . Experimentally, B_M is obtained from *macroscopic* measurements, such as polarization ones³; B_M is negative as required by the first-order character of the transition. The *microscopic* isothermal responses for modes propagating along $(1, 0, 0)$, and for

$$e_1 = \alpha P^2 + O(P^4), \quad e_3 = \beta P^2 + O(P^4), \quad e_6 = bP + O(P^3).$$

This is all one needs to evaluate $B_m - B_M$ and S/E :

$$B_m - B_M = \frac{8}{3}[(C_{11} + C_{12})\alpha^2 + \frac{1}{2}C_{33}\beta^2 + 2C_{13}\alpha\beta] - \frac{4}{3}(1/C_{11})[(C_{11} + C_{12})\alpha + C_{13}\beta]^2, \quad (3)$$

$$S/E = 2\sqrt{2}(C_{11} - C_{12})[(C_{11} + C_{12})\alpha + C_{13}\beta]b/C_{11}a^2(T - T_a)^2 + O(E^2). \quad (4)$$

Using the well-known elastic constants,¹² these equations give $B_m - B_M = 2.48 \times 10^{-11}$ esu and, at $T - T_a = 106$ mK, $S/E = 26.5$ esu/rad. From our measured B_m , one calculates $B_M = -1.76 \times 10^{-11}$ esu which falls within the most reliable experimental values.³ The calculated S/E (shown at $E = 0$, the limit for which it applies) also agrees excellently with measurements (Fig. 3). Hence, the expansion indicated here accounts quantitatively and without adjustable parameter for our surprising intensity results.

The qualitative implications of this agreement are even more striking. Were α and β zero, one would have $B_m = B_M$ and there would be opalescence. In other words, the deformations e_1 and e_3 play an *essential* role: As no acoustic wave exists that carries these deformations and e_6 simultaneously, there is no soft-acoustic wave for $E \neq 0$.⁶ Furthermore, any fluctuation in polarization or temperature also couples to strain when $E \neq 0$. Hence, there are no *microscopic* critical fluctuations and no diverging correlation length in the symmetry-nonbreaking transition. Landau theory should then apply strictly! It predicts classical divergences of macroscopic thermodynamic quantities: The isothermal free electric susceptibility $\chi_{T,\sigma}$, the free specific heat at constant field $C_{E,\sigma}$, and the compressibility given by determinant $|C_{ij}^0|^{-1}$, ($i, j = 1$ to 3), where the C_{ij}^0 's are isothermal orthorhombic elastic constants at constant field. The critical exponent at K is $-\frac{2}{3}$, whereas for approach to the spinodals from the metastable side it is $-\frac{1}{2}$. The latter might also be measurable, as it should be easy to penetrate deeply into the metastable region in large, perfect crystals. Our experi-

ments indicate a hysteresis of more than 100 mK for $E = 0$.¹⁰ small θ along $(1, \theta/\sqrt{2}, 0)$ have also been calculated, expressing the six strains in terms of the three independent displacements and obtaining the generalized susceptibility. The inverse of the resulting dielectric susceptibility is simply the right-hand side of Eq. (1), so that an explicit expression for B_m also results. The algebra is heavy but straightforward.¹¹ Many parameters are not known, but fortunately the result of the minimization $\partial G/\partial e_i = 0$ is *experimentally* available¹⁰:

ments indicate a hysteresis of more than 100 mK for $E = 0$.

Landau-like elastic transitions are generally expected in all symmetry-nonbreaking cases.¹³ They have already been discussed in relation to the "gas-liquid" transition of H dissolved in metals.¹⁴ A bulk-modulus instability was also reported for mixed-valence metallic alloys.¹⁵ Elastic effects should also play an important role in "real" crystals in which the high-temperature symmetry is broken by localized defects.

The authors gratefully acknowledge the technical assistance of H. Amrein, and fruitful discussions with A. Bruce, who critically commented on the manuscript, and with H. Thomas, who also pointed out Ref. 13.

^(a)Permanent address: Institute of Physical Science and Technology, University of Maryland, College Park, Md. 20742.

^(b)Present address: The Racah Institute of Physics, Hebrew University, Jerusalem, Israel.

¹B. A. Strukov, M. A. Korzhuev, A. Baddur, and V. A. Koptsik, *Fiz. Tverd. Tela* **13**, 1872 (1971) [*Sov. Phys. Solid State* **13**, 1569 (1972)].

²N. Lagakos and H. Z. Cummins, *Phys. Rev. B* **10**, 1063 (1974).

³A. B. Western, A. G. Baker, C. R. Bacon, and V. H. Schmidt, *Phys. Rev. B* **17**, 4461 (1978).

⁴M. de Quervain, *Helv. Phys. Acta* **17**, 509 (1944); A. von Arx and W. Bantle, *Helv. Phys. Acta* **17**, 298 (1944). Also cited by F. Jona and G. Shirane, in *Ferroelectric Crystals* (Pergamon, Oxford, 1962), pp. 68-72.

⁵E. M. Brody and H. Z. Cummins, *Phys. Rev. B* **9**

179 (1974).

⁶R. A. Cowley, Phys. Rev. B **13**, 4877 (1976).

⁷E. Courtens, Phys. Rev. Lett. **41**, 17 (1978). The same crystal was used here.

⁸As predicted by E. Pytte and H. Thomas, Solid State Commun. **11**, 161 (1972), and as observed in the FE phase by M. D. Mermelstein and H. Z. Cummins, Phys. Rev. B **16**, 2177 (1977).

⁹See Pytte and Thomas, Ref. 8.

¹⁰F. Jona and G. Shirane, Ref. 4; $\alpha = 3.84 \times 10^{12}$, $\beta = 2.9 \times 10^{-12}$, and $b = 5.0 \times 10^{-7}$, in cgs units.

¹¹E. Courtens, R. Gammon, and S. Alexander, to be published.

¹²S. Haussühl, Z. Kristallogr., Kristallgeom., Kristallphys., Kristallchem. **120**, 401 (1964).

¹³Symmetry-breaking continuous elastic transitions always have a soft elastic wave as shown by S. Aubry and R. Pick, J. Phys. (Paris) **32**, 657 (1971).

¹⁴H. Wagner and H. Horner, Adv. Phys. **23**, 587 (1974).

¹⁵R. L. Melcher, G. Guntherodt, T. Penney and F. Holtzberg, IEEE Trans. Sonics Ultrason. **23**, 205 (1976).

Vacancies and the Chemical Trapping of Hydrogen in Silicon

H. J. Stein

Sandia Laboratories, Albuquerque, New Mexico 87185

(Received 9 July 1979)

The first evidence for SiH₁-like centers in crystalline Si (*c*-Si) is presented from infrared measurements of H (D) implanted at 80 K. In contrast to SiH₁ centers in amorphous Si (*a*-Si) which are stable to ≈ 700 K, the crystalline band anneals below 300 K with an activation energy and illumination enhancement that are characteristic of the Si vacancy. These results relate specific defects for implanted H in *c*-Si to previous observations for H in *a*-Si.

Hydrogen bonds chemically in both crystalline Si (*c*-Si)^{1,2} and amorphous Si (*a*-Si)³ and produces significant changes in electrical properties.⁴ There is, however, little understanding of structural changes which accompany hydrogenation of Si. Understanding the relationships between structural composition and chemical bonding of hydrogen in Si is a necessary part of understanding electrical properties of hydrogenated Si. Hydrogen implantation into *c*-Si at 300 K produces a complex SiH stretch-frequency spectrum of at least twelve infrared absorption bands.^{1,2} Because these absorption bands have different annealing characteristics,^{1,2} they represent discrete SiH centers. However, since nuclear reaction-channeling analysis⁵ shows that a major fraction of hydrogen implanted into *c*-Si at 300 K occupies a well-defined crystalline interstitial site, it was suggested^{1,5} that the many SiH stretch frequencies in implanted *c*-Si are associated with different atomic-displacement-produced defects surrounding a well-defined interstitial hydrogen position within the crystalline lattice.⁵ In contrast to the many SiH bands produced by H implantation into *c*-Si at 300 K, implantation into *a*-Si yields a single broad band⁶ which has been assigned to the one-hydrogen (SiH₁) center.³

Reported herein are results obtained from studies on SiH stretch frequencies for hydrogen implanted into crystalline Si at low temperature. From these results one can infer that low-temperature. From these results one can infer that low-temperature H implantation into *c*-Si produces Si-H bonding similar to the SiH₁ bonding observed in *a*-Si. In addition, from the annealing studies reported here, one can relate the loss of this band to the motion of the Si vacancy in *c*-Si.

Hydrogen implantations of 6×10^{15} cm⁻² were made at 50 and 100 keV at 80 K into both 0.63 \times 1.27 cm² faces of high-resistivity (111) samples of *n*-type crucible-grown Si. The penetration depth for 100-keV hydrogen into Si is 1 μ m; therefore, the average concentration within an implanted layer is $\sim 1.2 \times 10^{20}$ H/cm³.

The solid trace in Fig. 1 shows the SiH absorption spectrum produced by H implantation into *c*-Si at 80 K. This spectrum is much less complex than that for implantation at 300 K. The major SiH stretch frequency at 1990 cm⁻¹ observed after low-temperature implantation of hydrogen into⁷ *c*-Si is essentially the same as that for the SiH₁ centers produced by implantation into *a*-Si at 300 K (dotted trace of Fig. 1). An